Intracardiac Catheter 2-D Arrays on a Silicon Substrate

Warren Lee, *Student Member, IEEE*, and Stephen W. Smith, *Member, IEEE*

***Abstract*—The design, fabrication, and characterization of a 7 MHz, two-dimensional (2-D) array transducer built on a silicon substrate is described. The array fits inside a 9-French (2.9 mm O.D.) catheter for use in real-time intracardiac volumetric imaging. The −6 dB fractional bandwidth of the transducer is 30%, the 50 Ω pitch-catch insertion loss is 78 dB, and the interelement crosstalk is −25 dB. Real-time volumetric images in phantoms and in-vitro images of a sheep heart have been acquired yielding measured spatial resolution of 2 mm at a depth of 1 cm. The cardiac structures imaged include ventricular chambers, interventricular septum, mitral and tricuspid valves and real-time 3-D rendered volumes of the tricuspid valve in the open and closed position.**

I. Introduction

Recently , much attention has been devoted to the development of miniaturized, catheter-based transducers suitable for intracardiac ultrasound imaging. This new research interest has been spurred by the potential advantages that intracardiac imaging affords over conventional transthoracic ultrasound imaging and x-ray fluoroscopy. Advantages over transthoracic ultrasound imaging may include improved visualization of certain cardiac structures due to the lack of acoustic barriers presented by the chest wall and lungs. For example, these acoustic barriers, along with the orientation of the heart, cause the atria to be far removed from the acoustic window available from outside the body. Thus, structures within the atrium are poorly resolved using the transthoracic approach. The intracardiac approach is advantageous due to the closer proximity of the transducer to the cardiac structures of interest. The reduction in required penetration depth allows a higher operating frequency to be used due to the reduced effects of frequency-dependent attenuation and may lead to a direct improvement in spatial resolution. In addition, intracardiac ultrasound imaging may be used as an alternative to x-ray fluoroscopy imaging during cardiac interventional procedures with advantages, including the improved visualization of soft tissues, increased accuracy in ablation site placement [1], visualization and measurement of ablated tissue [2], and the lack of exposure to ionizing radiation. Also, intracardiac echocardiography (ICE) may offer an advantage over transesophageal imaging, which often requires general anesthesia for extended interventional procedures, thus posing disadvantages in terms of health risk and cost. Currently, there are two commercial catheter-based intracardiac probes used for clinical ultrasound B-scan imaging: A 9 F, 9 MHz rotating single-element catheter (EP Technologies, Boston Scientific Corp, San Jose, CA) [3], and A 10 F, 5.5–10 MHz, phased-array ultrasound catheter (Acuson Corp, Mountain View, CA) [4].

Although these intracardiac transducers can be used to aid in the guidance of interventional cardiac procedures, both have limitations associated with the monoplanar nature of the B-scan images. Real-time 3-D (volumetric) imaging is a natural extension in the advancement of intracardiac imaging. In real-time volumetric imaging, a 2-D array transducer is used to steer and focus the ultrasound beam over a pyramidal shaped volume rather than a single sector scan [5], [6]. In real-time volumetric intracardiac imaging, a miniature 2-D transducer is inserted into the heart, enabling the 3-D viewing of cardiac structures and interventional catheter devices in cross sectional and en face views as well as real-time 3-D rendered images [7]. Multiple real-time B, C, or inclined planes can be displayed, as well as real-time 3-D rendered images [8].

We previously described 5.0 MHz catheter 2-D arrays for intracardiac applications with an interelement spacing of 200 μm [9], [10]. The transducer arrays were fabricated on a six-layer flexible polyimide interconnect circuit with 25 μm wide traces. The transducer assemblies fit inside 12-French (12 F) (3.8 mm O.D) catheters using standard micro-coaxial cables. This design has been used in animal experiments to show the potential of intracardiac volumetric scanning [8], but the 12 F catheter size is too large to be clinically useful. In this paper we describe a new catheter 2-D array design that can be extended to higher operating frequencies, and smaller, more clinically useful catheter sizes. However, as we move toward higher operating frequencies, the feature sizes of the catheter 2-D array decrease significantly, complicating their construction.

The new catheter operated at a nominal frequency of 7 MHz, with an interelement spacing of 150 μm, and fit inside of a 9 F catheter. The smaller feature sizes required in the 9 F design precluded the use of a flexible substrate due to tolerances in the fabrication processes of our source for the flex circuit interconnect. Instead, the polyimide interconnects were constructed on a silicon substrate using thin film photolithography processing techniques. The use of silicon substrates have been described for several types of transducers, including integrated silicon-PVDF trans-

Manuscript received March 7, 2001; accepted November 14, 2001. This research was supported in part by NIH grants HL 64962 and HL 58754.

The authors are with the Department of Biomedical Engineering, Duke University, Durham, NC 27708-0281 (e-mail: warren.lee@duke.edu).

ducers [11], [12], acoustic camera arrays [13], and micromachined capacitor arrays [14], [15]. Silicon-based IC processing allows for the efficient batch production of transducers, and the silicon can be beneficial in the fabrication of transducers due to the uniformity in the surface flatness of the silicon wafer substrate. However, the presence of the silicon wafer in the transducer backing may pose a disadvantage from an acoustical standpoint, resulting in a reduced bandwidth. Our hypothesis is that, although the presence of silicon in the transducer backing decreases the bandwidth of the transducer, the spatial resolution is still sufficient to obtain potentially useful intracardiac images. In this paper we describe the design, fabrication, and experimental results of a catheter 2-D array on a silicon substrate, including images of phantoms as well as images of an in-vitro sheep heart.

II. Methods

A. Design and Simulation

The primary design constraint of our catheter 2-D array arose from the number of signal cables that physically fit inside the catheter. The inner diameter of our 9 F catheter was 2.1 mm. Given this size constraint, we used a prototype "virtual coaxial cable" [16] developed by Precision Interconnect (Portland, OR) which enabled 70 cables to fit inside the 9 F catheter. The proprietary virtual coaxial cables may achieve low capacitance and acceptable cross talk without the need for an individual shield on each of the insulated conductors, allowing for a high density of signal conductors in a small, flexible cable assembly. The insulated signal cables are arranged in layers of concentric rows, and they are capacitively coupled to concentric conducting shields, which encircle each row. At least one uninsulated conductor is present in each row so that the concentric shields between rows are at an equipotential. The rows are wound in a helical shape around an uninsulated, high tensile strength center conductor that may serve as a strain relief.

The overall dimensions of the 2-D array were determined by space constraints within the 9 F catheter lumen, and the packing density of the virtual coax determined the number of active elements. Given these constraints, an operating frequency of 7 MHz was selected, which then determined the physical dimensions of each 2-D array element, due to grating lobe and resonance mode considerations. For 70 active channels, we could achieve an interelement spacing of 0.15 mm, which is less than a wavelength in tissue for our design frequency of 7 MHz ($\lambda = 0.21$ mm). The lead zirconate titanate (PZT) thickness necessary for a resonant frequency of 7 MHz was determined to be 0.18 mm. With a saw kerf width of 0.03 mm, the element width and length are 0.12 mm. The resulting width-to-thickness ratio = 0.67 was sufficiently small to decouple the width and length mode resonances from the desired thickness mode resonance. The physical dimensions of the 2-D array element are summarized in Table I.

TABLE I
The 2-D Array Element Parameters.

Quantity	Symbol	Value
Nominal frequency	f_o	7 MHz
Interelement spacing	d	0.15 mm
Element Thickness	t	0.18 mm
Element width	w	0.12 mm
Width/thickness ratio	w/t	0.67
Element length	l	0.12 mm
Length/thickness ratio	l/t	0.67

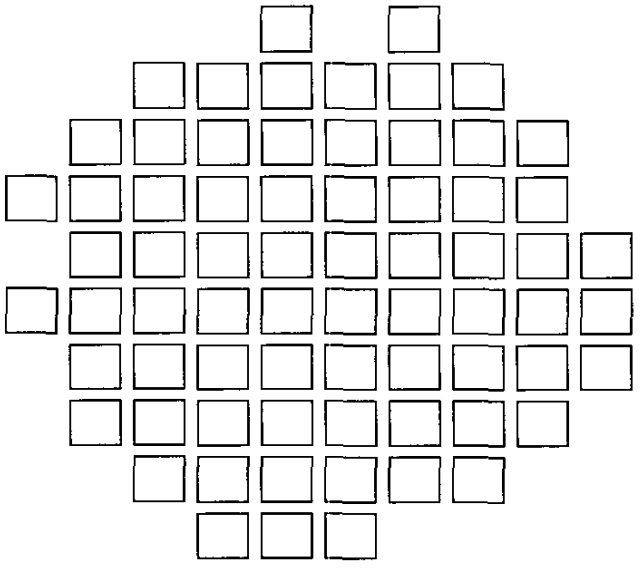

Fig. 1. 2-D array geometry.

Field II software developed by Jensen and Svendsen [17] was used to model the characteristics of the beam shape resulting from different array geometries. The simulations used a Gaussian-shaped pulse centered at 7 MHz with a −6 dB fractional bandwidth of 30%. Because the small size of 2-D array elements results in a low sensitivity, only those transducer geometries that utilized all 70 available channels in both transmit and receive were considered. The array geometry illustrated in Fig. 1 showed desirable results in terms of sensitivity, main lobe width and off-axis clutter.

The size of the aperture is approximately 1.5 mm. Fig. 2(a) shows the calculated on-axis, pulse-echo beam response vs. angle for the selected array geometry. The −6 dB and −20 dB beam widths are approximately 9° and 15°, respectively. A clutter floor is present at a level of −50 dB for angles greater than ±25°. Fig. 2(b) shows the −6 dB and −20 dB beamwidths in millimeters. vs. depth for the transducer. We note that, at a depth of 1 cm, the −6 dB and −20 dB beamwidths are 1.5 mm and 2.8 mm, respectively. This implies that, at short ranges, the spatial resolution should be adequate to resolve important cardiac structures.

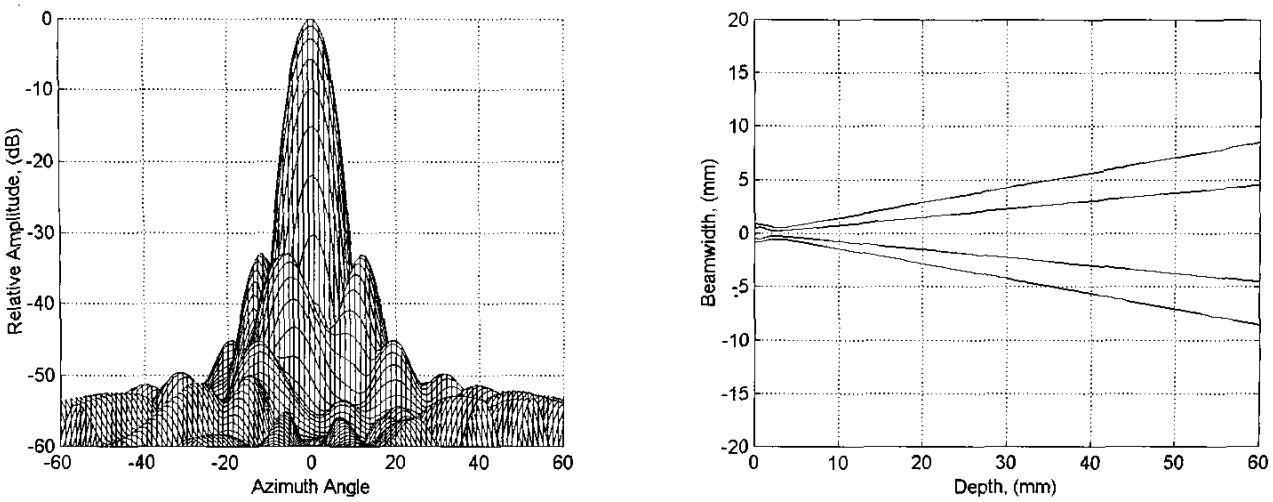

Fig. 2. Field II simulation results: Pulse-echo beamplots (a), on-axis beamplot (b) −6 dB and −20 dB beamwidths in millimeters vs. depth.

TABLE II
THE KLM SIMULATION PARAMETERS FOR THE CASE WITH SILICON.

Layer Description	Long. velocity (m/s)	Density (kg/m^3)	Loss (dB/cm)	Thickness (mm)
Silver foil	3600	10500	0.0	0.007
Silver epoxy	1900	2684	8.0	0.030
PZT 5H ($k_t = 0.755$)	3850	7500	elec. loss tan. = 0.02 mech. loss tan. = 0.015	0.180
Silver epoxy	1900	2684	8.0	0.030
Polyimide substrate	2200	1409	0.0	0.012
Silicon	8439	2340	0.0	0.600
Acoustic backing	2450	1100	54.0	1.000
Nylon catheter	2770	1140	3.2	0.400

The Krimholtz, Leedom, and Matthaei (KLM) model [18] can be used to simulate the thickness-mode resonant behavior of a 2-D array element. Simulations were performed with and without a silicon substrate in the transducer backing to determine its effects on transducer performance. Table II lists the simulation parameters for the transducer with silicon in the backing. The modeled layers and their thicknesses are shown in Fig. 3. Internal layers of the flex circuit were not included in the model. The silver epoxy bond on the front of the PZT provided some degree of acoustic matching. The parameters for the case without silicon in the backing were the same, with the exception that the thickness of the silicon was replaced with an equivalent thickness of additional acoustic backing. The simulations included a 50 Ω transmitter output impedance, 20 kΩ receiver input impedance. A 36 pF shunt capacitance represented the virtual coaxial cable assuming a nominal shunt capacitance of 12 pF/ft.

The simulated pulse-echo impulse response and power spectrum for the cases with and without silicon are shown in Fig. 4. The peak frequency for the transducer is 6.3 MHz and 6.1 MHz for the two cases, respectively. Results indicate that the presence of the silicon would decrease the −6 dB fractional bandwidth from 33% to 16%. The resonance present at 2.5 MHz could be due to a $\lambda/4$ mechanical resonance in the silicon substrate.

B. Interconnect Fabrication

The six-layer interconnect circuit was fabricated at North Carolina State University and has been described in detail by Fiering *et al.* [10]. Briefly, a thin film of polyimide was spin cast and cured onto a thermally oxidized silicon wafer. The signal and ground layers were each formed by the patterning and etching of sputtered thin-film gold yielding 12 μm traces spaced 12 μm apart. Intermediate dielectric layers were formed by spin coating polyimide. A laminated layer of DuPont Pyralux (Wilmington, DE) served a stand-off to prevent the cutting of circuit traces during dicing of the PZT. The topmost metal layer consisted of electroplated copper solder pads for wiring connections to the virtual coax cables and contact pads for connecting to individual PZT elements. Connections between layers throughout the interconnect were achieved with photo-defined stepped vias. Fig. 5 shows a top view of the multilayer interconnect on the silicon substrate, and

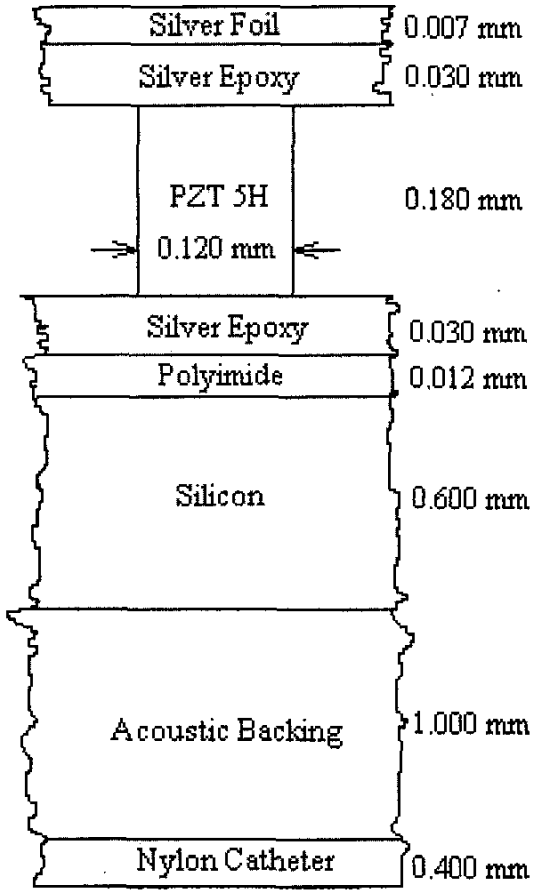

Fig. 3. KLM modeled layers and thicknesses.

a cross section showing the layers of the interconnect circuit is given in Fig. 6. The 70 active elements at the array end were electrically connected to the coax solder pads by traces running lengthwise in the signal layer of the interconnect. Thickness dimensions of the interconnect circuit are given in the Table III. The interconnect circuit had 14 rows of 5 solder pads at 0.38 mm pitch alternating with ground buses, and was 2.1 mm wide by 49.5 mm long.

C. Transducer Fabrication

Fabrication of the transducer on the multilayer interconnect circuit has been described previously [19] and will be summarized here. First, PZT was bonded to the interconnect using conductive silver epoxy (Part # 50-10-0584-0029, Chomerics, Woburn, MA). The individual elements were formed by dicing with a diamond dicing saw (Model 780, Kulicke and Soffa, Willow Grove, PA), with the saw kerf extending through the PZT into the laminated layer of Pyralux, but not into the ground or trace layers beneath. A closeup of the diced array on the interconnect circuit is shown in Fig. 7. Silver epoxy was then used to bond a thin silver foil to the top of the PZT elements to serve as the ground electrode. The transducer and flex circuit assembly were sent to Precision Interconnect (PI, Wilsonville, OR) where cable connections were made to each solder pad using virtual coax. The 70 virtual coax cables were fed through 3 feet of 9 F catheter, and were terminated into a PI PAC connector at the proximal end, which in turn led through the system cable assembly and ITT Canon Model DLM6-360P (White Plains, NY) connector, and into the volumetric scanner. The wired transducer then was pulled into the catheter lumen, where a window was cut out of the catheter wall so that the catheter had a side scanning orientation. A loaded epoxy acoustic backing was injected into the lumen of the catheter behind the transducer array. The tip of the catheter, including the transducer, was then coated with an acrylic polymer to protect it from the environment.

TABLE III
INTERCONNECT THICKNESS DIMENSIONS.

Layer	Thickness (μm)
Silicon wafer	600
Polyimide substrate	12
Cr/Au traces	0.5
Pyralin dielectric	2
Cr/Au ground layer	0.2
Pyralin dielectric	2
Pyralux dielectric	25
Cr/Au/Cu contact pads	5
Total Thickness	647

D. Measurements

The impulse response and power spectrum, 50 Ω insertion loss, and interelement crosstalk were measured in order to characterize the transducer. The impulse response was obtained by transmitting with a Metrotek Model 215 transmitter (St. Petersburg, FL) and observing the reflection from an aluminum block with a 10 pf Tektronix probe (Wilsonville, OR) into a Tektronix Model TDS744A Digitizing Oscilloscope. The spectrum was obtained using a Panametrics 5052G Stepless Gate (Waltham, MA) and a Hewlett-Packard Model 3588A Spectrum Analyzer (Palo Alto, CA).

The 50 Ω pitch-catch insertion loss was measured using a Hewlett-Packard Model 8165A Programmable Signal Source Generator and an ENI model 325LA RF Power Amplifier (Rochester, NY) with a 50 Ω output impedance to generate a 10-cycle burst at the desired frequency on a transmit element. An aluminum block at a range of 5 mm was used to reflect the transmitted signal into a receive element loaded by a scope probe with an input impedance of 50 Ω.

Interelement crosstalk measurements were made by transmitting on a single element and measuring the crosstalk on adjacent elements, with the transducer in a water tank. The elements were loaded with the virtual coax cable and the system cable, and terminated with 60 pF in parallel with 20 kΩ to simulate system loading. In order to obtain a worst-case scenario, the crosstalk was measured

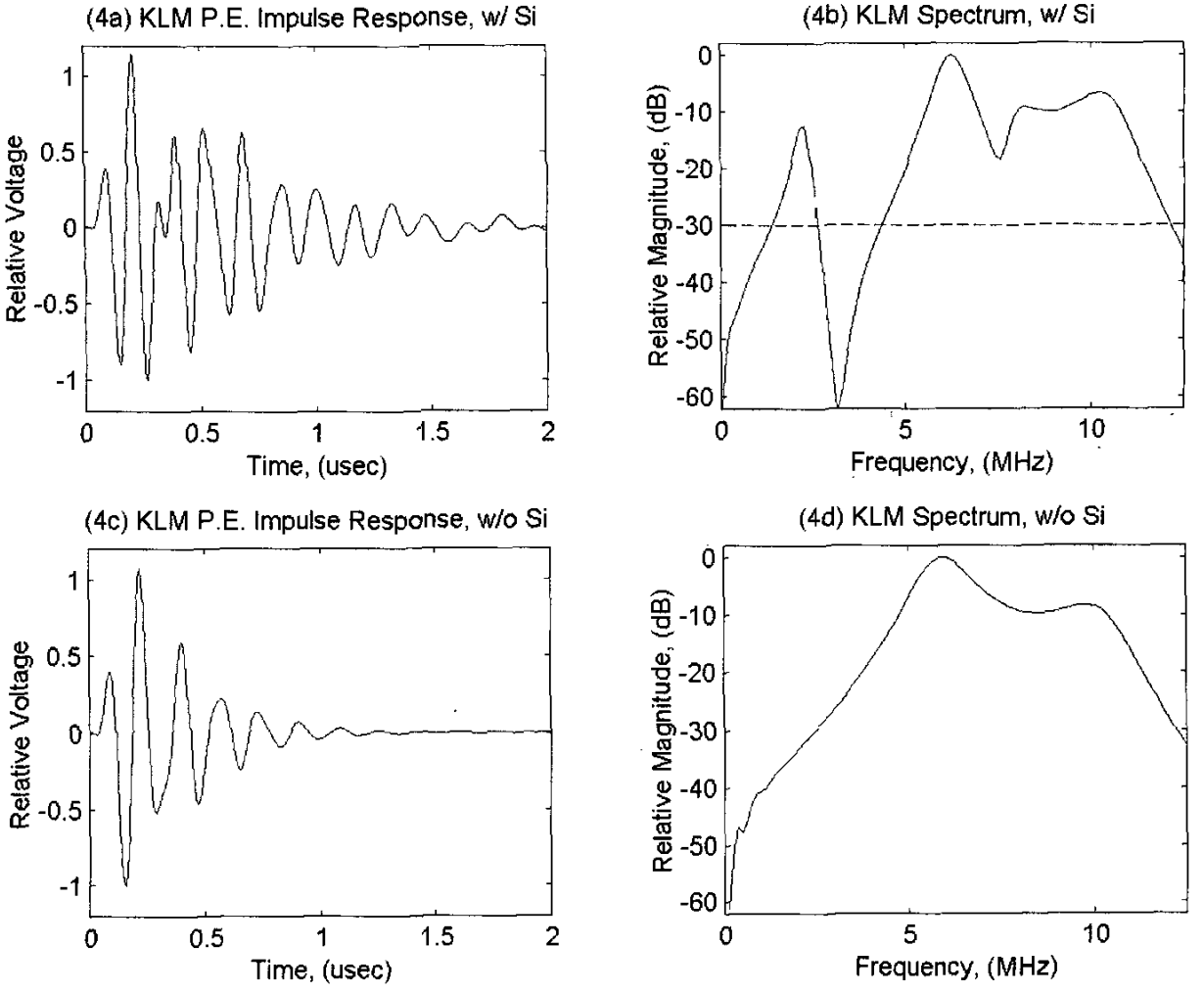

Fig. 4. KLM simulation results: (a) and (b) impulse response and spectrum for the silicon case, (c) and (d) for the case without silicon.

TABLE IV
TRANSDUCER CHARACTERIZATION RESULTS.

Transducer	Peak frequency	−6 dB fractional bandwidth	50 Ω insertion loss	Crosstalk
7.0 MHz 2-D catheter array	6.6 MHz	30%	78 dB	−25 dB

for several different elements, including those adjacent to the transmit channel on the array, the PI PAC connector, and ITT Canon system connector.

III. RESULTS

A. Transducer Characterization Results

Results of the transducer characterization tests are summarized in Table IV: The 50 Ω insertion loss of 78 dB is greater than the 64 dB we previously reported for our 5 MHz, 12 F catheter 2-D arrays [10] as the current transducer assembly could be tested only after connecting the 3 feet of virtual coax cable. The KLM simulations indicate that discounting the cable brings the insertion loss in line with previous measurements.

The −25 dB crosstalk measurement is similar to results reported for our previous 2-D arrays that utilized conventional micro-coaxial cables, indicating that the dominant source of crosstalk may not be due to the virtual coaxial catheter cable, but may be due to other interconnections within the total assembly, such as the flex circuit, ITT Canon system connector, or the PI PAC connector.

An illustrative pitch-catch pulse and spectrum are shown in Fig. 8. These are in reasonable agreement with the KLM simulations of Fig. 4 considering the approximations used for the flex circuit and virtual coax cable in

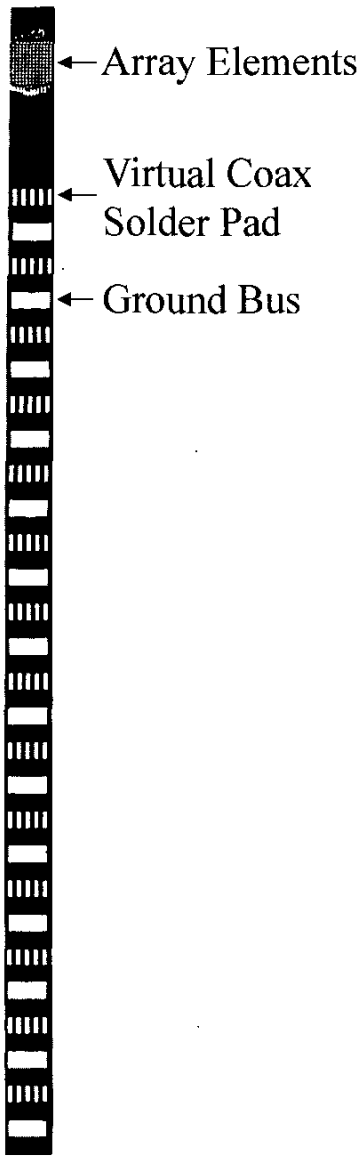

Fig. 5. Multilayer polyimide interconnect circuit on silicon substrate (top view), showing array elements and 14 rows of 5 solder pads each, alternating with ground buses.

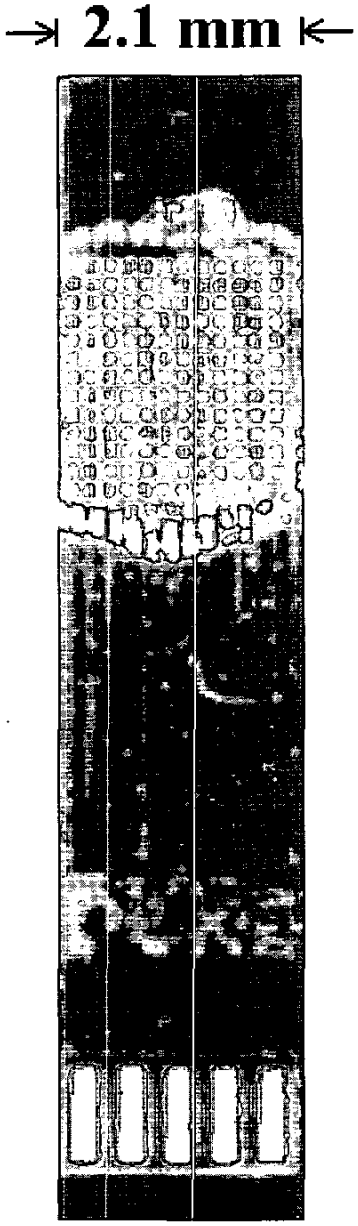

Fig. 7. Close-up of the diced array and first row of coaxial cable solder pads.

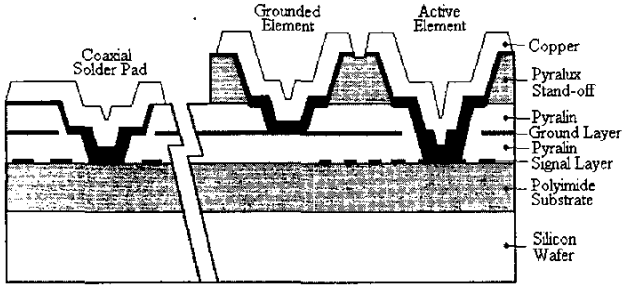

Fig. 6. Longitudinal cross-sectional schematic of the interconnect circuit, showing individual layers.

modeling the transducer. Note the dashed line in Fig. 4(b) corresponds to the noise floor of the experimental spectrum in Fig. 8(b). From the experimental spectrum, we see the peak frequency response at 6.6 MHz and a secondary peak at approximately 2.5 MHz, possibly caused by a quarter-wave resonance in the silicon as in the KLM model. The phase inversion at 0.35 μs present in the KLM simulations in Fig. 4(a) is absent from the experimental pulse in Fig. 8(a). We also note that the experimentally measured -6 dB fractional bandwidth of the transducer on the silicon substrate was 30%, as compared to 16% in the KLM simulations. This 30% experimental bandwidth may have been caused by the silver epoxy layer on top of

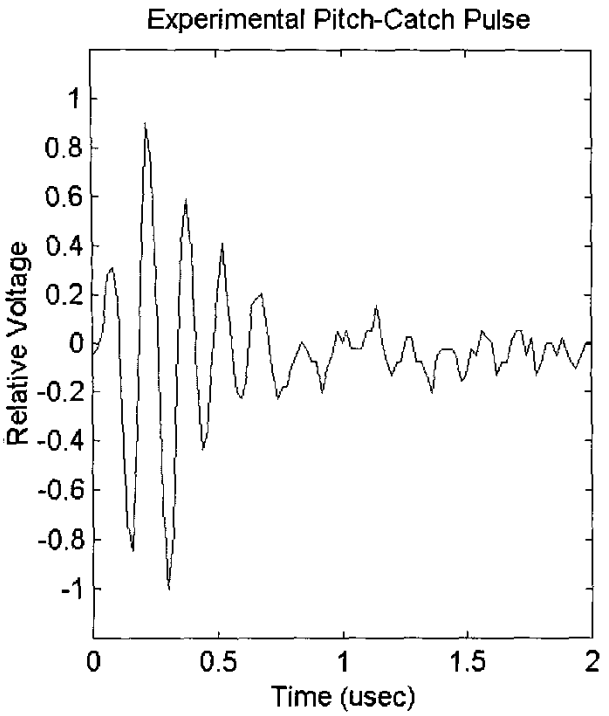

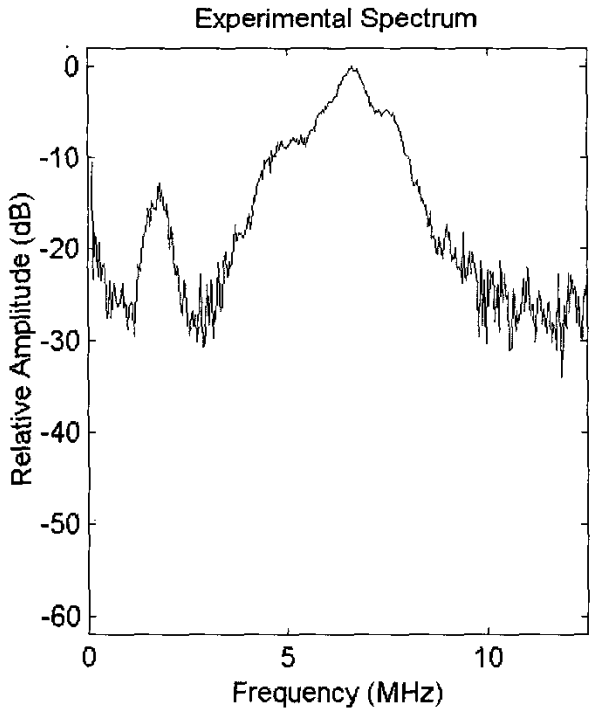

Fig. 8. Experimental pitch-catch pulse (a) and spectrum (b).

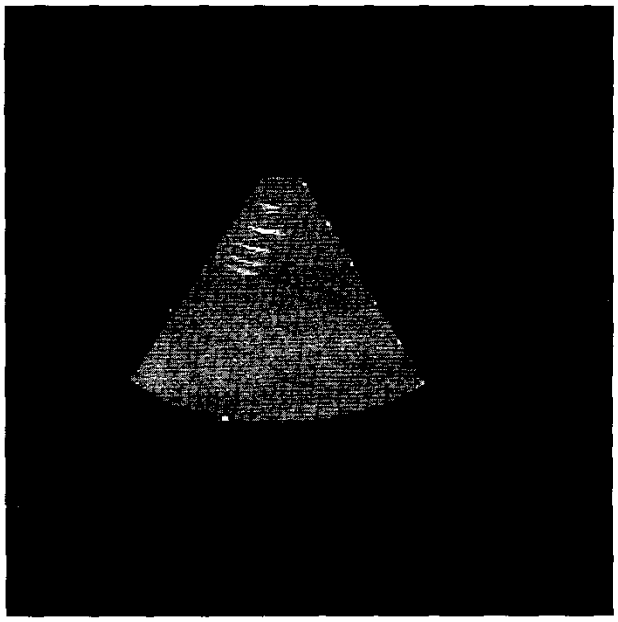

Fig. 9. B-scan image of AIUM 100 mm test phantom demonstrating axial resolution.

the array acting as a better matching layer than initially anticipated.

B. Images

Using the Model I scanner developed by Volumetrics Medical Imaging (Durham, NC), we obtained real time 3-D scans of phantoms and excised tissue. Twelve bit dynamic range was available at the detector input.

Fig. 9 shows an image of six axial resolution targets in water from the AIUM 100 mm test phantom separated by 5, 4, 3, 2, and 1 mm. The catheter 2-D array is able to resolve five of the wires. The scale markers to the right of each B-scan indicate 1 cm increments in the 6 cm scan. Fig. 10(a) shows a B-scan of the same AIUM targets tilted in an orientation more indicative of lateral resolution. The tilted C-scan shown in Fig. 10(b) is taken in a cut indicated by the arrows in Fig. 10(a). Again, our transducer resolves five of the six wires in both the B- and C-scans, indicating spatial resolution of 2 mm in both axial and lateral directions.

Figs. 11(a) and (b) shows B- and tilted C-scans of a 4 mm diameter hole drilled in a 2 cm thick sponge. The sponge is at a distance of 1 cm from the transducer, and the hole is resolved in both the B- and C-scans. Figs. 11(c) and (d) show B- and C-scans of a 2.5-mm diameter hole in a sponge. Again, the sponge is at a distance of 1 cm away from the transducer, and the hole is resolved in both the B- and C-scans. We note that our ability to resolve the 2.5 mm hole at a depth of 1 cm is consistent with the results of the beamwidth vs. depth simulations shown in Fig. 2(b), which indicate that the -6 dB and -20 dB

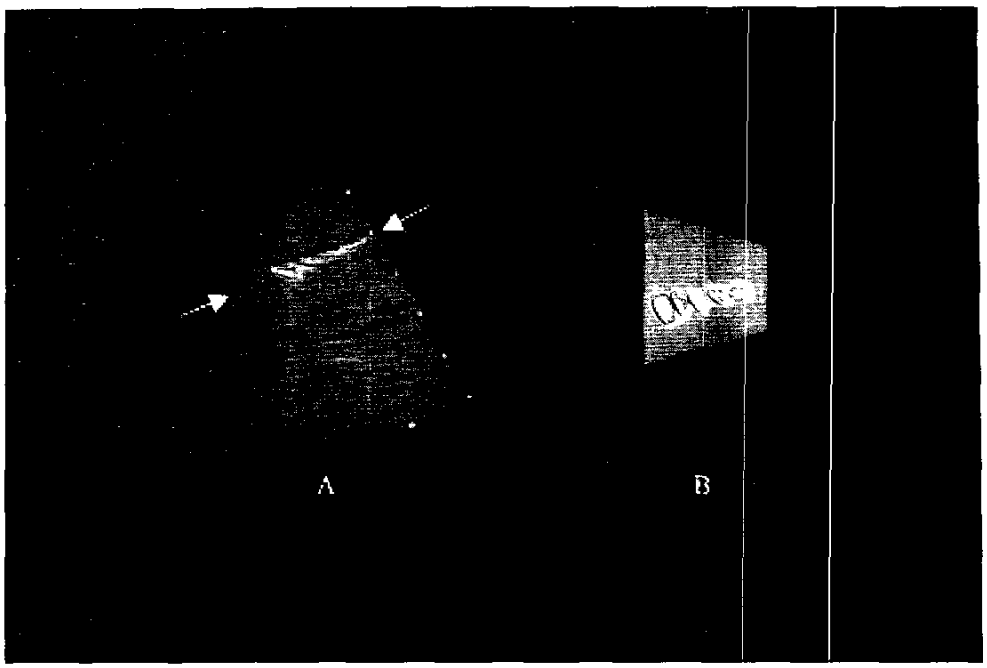

Fig. 10. AIUM 100 mm test phantom images: (a) B-scan demonstrating lateral resolution, (b) C-scan taken at the arrows indicated on the B-scan.

beamwidths at a depth of 1 cm are 1.5 mm and 2.8 mm, respectively.

Figs. 12(a) and (b) show orthogonal B-scans taken from an excised sheep heart preserved using a fixative formulation that maintains tissue flexibility [20]. Fig. 12(c) is the C-scan taken at the arrows indicated in the B-scans. All images were acquired simultaneously in real time. In the images, the catheter transducer is positioned in the left ventricle (LV), and the scan depth is 6 cm. We note the delineation of both the left ventricular and right ventricular (RV) chambers as well as the interventricular septum (S), and the right ventricular wall. The C-scan also shows the characteristic crescent shape of the right ventricle.

Figs. 13(a) and (b) show two orthogonal images of the sheep heart, with the catheter located in the apex of the left ventricle so that the mitral valve (M), and its separation of the left ventricle (LV) and atrium (LA) are distinguished. Fig. 13(c) is a tilted C-scan also showing the mitral valve and its separation of the left ventricle and atrium.

In Fig. 14, the transducer is positioned in the right ventricle (RV), and oriented such that the tricuspid valve (TV) and right atrium (RA) are imaged. Fig. 14(b) is a real-time, 3-D rendered image showing a portion of the tricuspid valve in the open position, and Fig. 14(c) is the same rendered image but with the tricuspid valve in the closed position. The opening and closing of the valve was accomplished by manually pumping the heart.

IV. Discussion

We have described the design, fabrication, and performance testing of a 9 F, catheter, 2-D array operating at 7 MHz for intracardiac volumetric scanning. The small size and high frequency of the transducer is consistent with commercial intracardiac ultrasound catheters now in clinical use with only B-scan capability. The reduced size of our catheter 2-D array is achieved through the use of a polyimide interconnect using thin film processing on a silicon substrate and a prototype virtual coax cable, which enables 70 transducer channels to fit in the 9 F lumen.

Limitations in the design mainly revolve around the presence of silicon in the transducer backing. One consequence of the silicon is an elongated impulse response and reduction in the fractional bandwidth of the transducer. However, real-time volumetric images of phantoms yield spatial resolution measurements of 2 mm for targets at short ranges. Volumetric images of an in-vitro sheep heart show common structures of cardiac anatomy that may be clinically useful in the guidance of interventional cardiac procedures.

Further improvements in the performance of the catheter array are under investigation, including improved acoustic matching layers. Another possibility to increase the bandwidth of the transducer array would be to mill out the silicon substrate using the diamond wheel dicing saw as the last step of the transducer fabrication process. The resulting area behind the transducer then could be filled with an acoustic backing. Removal of the silicon substrate using this milling process also would increase the flexibility at the distal end of the catheter where the interconnect

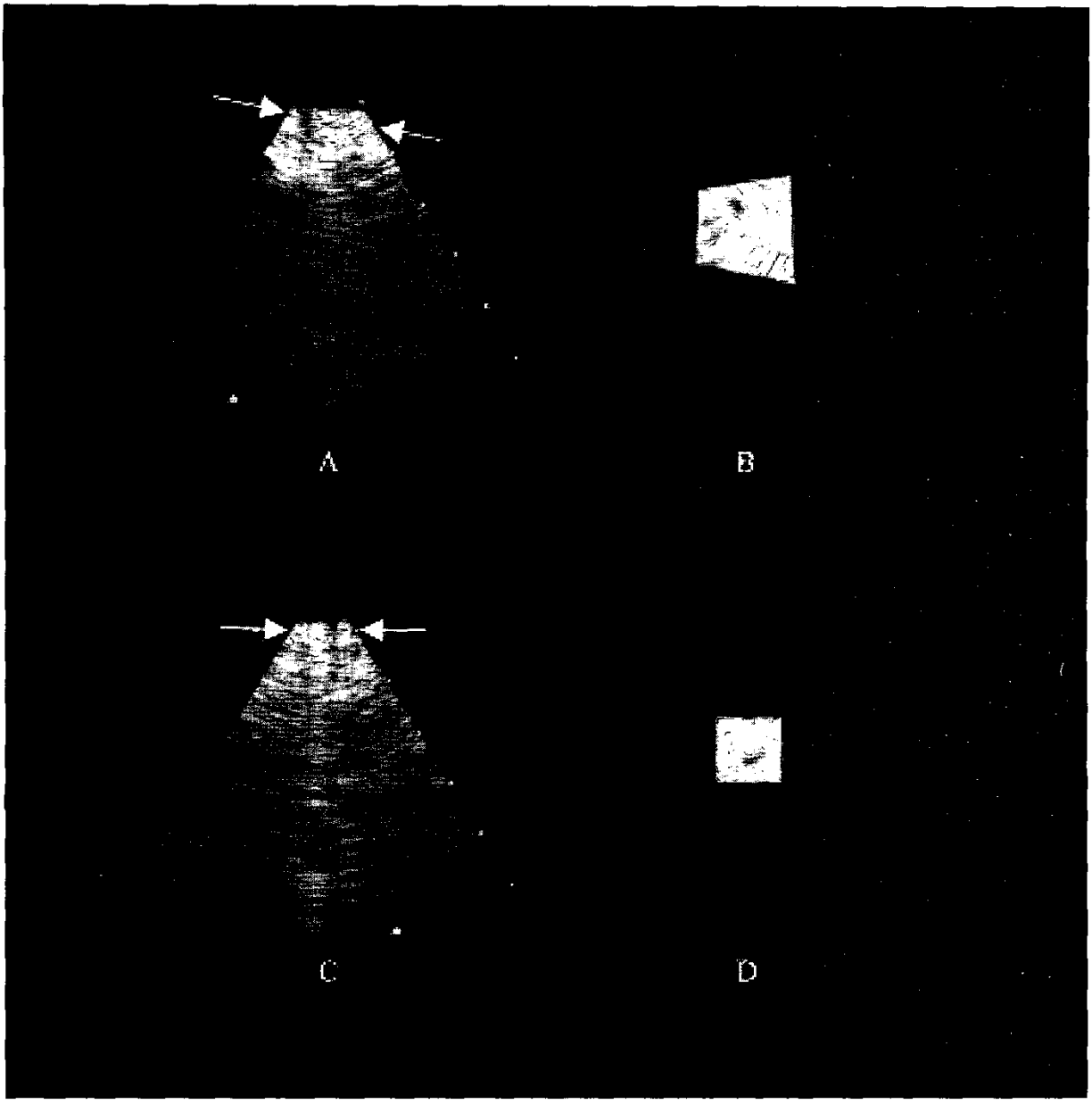

Fig. 11. Images of tissue-mimicking sponge phantom: (a) B-scan showing a 4 mm hole, (b) C-scan showing the 4 mm hole taken at the arrows indicated on the B-scan, (c) B-scan showing 2.5 mm hole, (d) C-scan showing the 2.5 mm hole.

circuit resides, and would lessen the fragility of the transducer.

Future work in catheter 2-D arrays for real-time intracardiac volumetric imaging involves moving to even higher operating frequencies to further improve the spatial resolution of the images while incorporating IC preamplifiers into the catheter to increase sensitivity. As even higher frequencies are employed, smaller feature sizes for the transducer are necessary and achievable with thin-film photolithographic processes on silicon. Other future work involves combining the diagnostic capabilities of intracardiac volumetric imaging with tools for therapeutic purposes. Examples include the integration of an optical fiber with the imaging array for delivery of laser radiation, useful in such procedures as percutaneous transmyocardial laser revascularization (PTMR) [21], [22]. Another possibility lies in the integration of the imaging array with a drug delivery mechanism that could deliver an angiogenic drug for patients suffering from coronary artery disease [23]. Such multifunctional catheters may reduce both the cost and the stress of cardiac interventions that currently require multiple catheters and the x-ray catheterization laboratory.

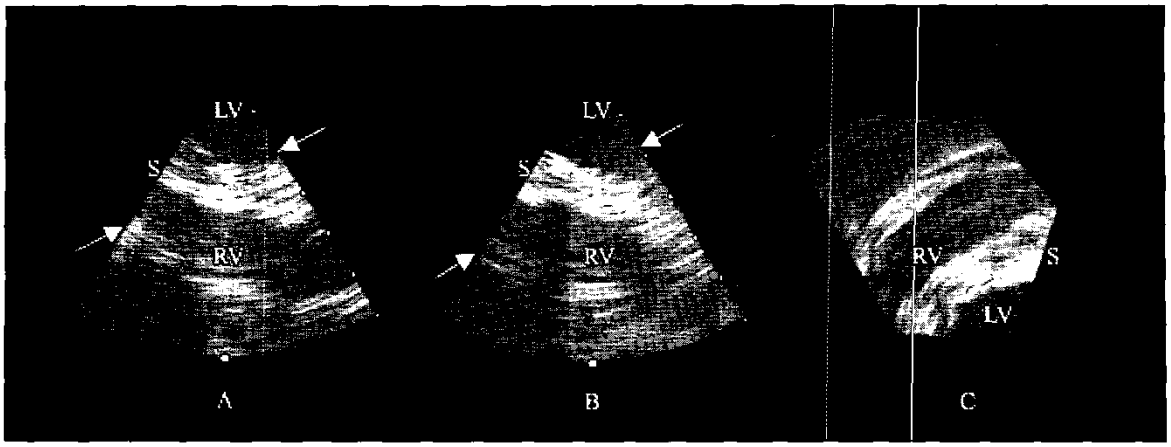

Fig. 12. In-vitro sheep heart images: (a) and (b) orthogonal B-scans with the imaging catheter in the left ventricle showing the left ventricle (LV), interventricular septum (S), and right ventricle (RV). (c) C-scan showing the crescent shape of the RV.

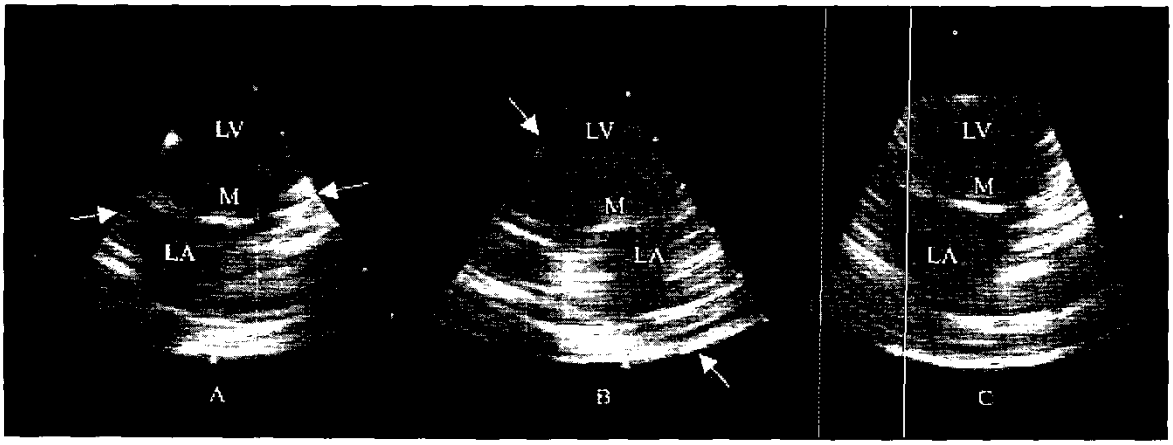

Fig. 13. In-vitro sheep heart images: (a) and (b) orthogonal B-scans with the catheter in the left ventricle, showing the left ventricular (LV) and atrial (LA) chambers separated by the mitral valve (M). (c) Tilted C-scan showing the same structures.

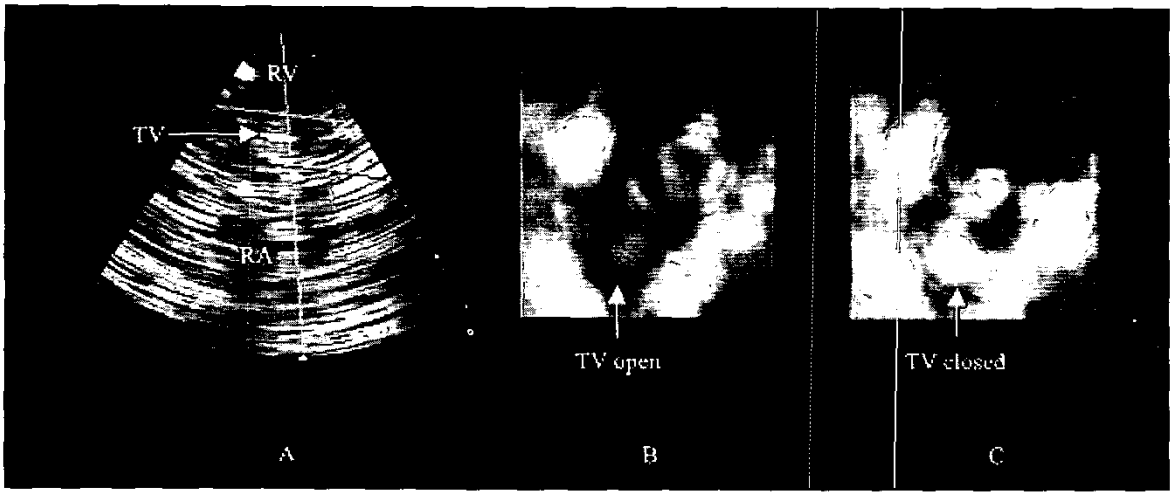

Fig. 14. In vitro sheep heart images: (a) catheter positioned in the right ventricle (RV), imaging the tricuspid valve (TV) and right atrium (RA). Real-time 3-D rendered imaged showing a portion of the tricuspid valve in the open position (b) and closed position (c).

ACKNOWLEDGMENTS

The authors would like to thank Precision Interconnect for providing integrated catheter packaging solutions, assembly expertise, termination processes, and cable technologies.

REFERENCES

[1] R. C. Chan, S. B. Johnson, J. B. Seward, and D. L. Packer, "Accuracy of intracardiac ultrasound assessment of RF ablation lesion dimensions in the intact canine atrium and ventricle," *Circulation*, vol. 92, (Suppl 1), pp. I–794, 1995, (Abst.).

[2] J. B. Seward, D. L. Packer, R. C. Chan, M. Curley, and A. J. Tajik, "Ultrasound cardioscopy: Embarking on a new journey," *Mayo Clin. Proc.*, vol. 71, pp. 629–635, 1996.

[3] E. Chu, A. P. Fitzpatrick, M. C. Chin, K. Sudhir, P. G. Yock, and M. D. Lesh, "Radiofrequency catheter ablation guided by intracardiac echocardiography," *Circulation*, vol. 89, pp. 1301–1305, 1994.

[4] C. J. Bruce, D. L. Packer, and J. B. Seward, "Intracardiac doppler hemodynamics and flow: New vector phased array ultrasound tipped catheter," *Amer. J. Cardiol.*, vol. 83, pp. 1509–1512, 1999.

[5] S. W. Smith, H. G. Pavy, and O. T. von Ramm, "High-speed ultrasound volumetric imaging system. Part I: Transducer design and beam steering," *IEEE Trans. Ultrason., Ferroelect., Freq. Contr.*, vol. 38, pp. 100–108, 1991.

[6] O. T. von Ramm, S. W. Smith, and H. G. Pavy, "High-speed ultrasound volumetric imaging system. Part II: Parallel processing and image display," *IEEE Trans. Ultrason., Ferroelect., Freq. Contr.*, vol. 38, pp. 109–115, 1991.

[7] E. D. Light, S. F. Idriss, P. D. Wolf, and S. W. Smith, "Real time three dimensional intracardiac echocardiography," *Ultrasound Med. Biol.*, .

[8] G. D. Stetten, T. Ota, and C. J. Ohazama, "Real-time 3-D ultrasound: A new look at the heart," *J. Cardiol. Diag. Proc.*, vol. 15, pp. 73–84, 1998.

[9] E. D. Light, R. E. Davidsen, J. O. Fiering, T. A. Hruschka, and S. W. Smith, "Progress in two-dimensional arrays for real-time volumetric imaging," *Ultrason. Imaging*, vol. 20, pp. 235–250, 1998.

[10] J. O. Fiering, P. Hultman, W. Lee, E. D. Light, and S. W. Smith, "High-density flexible interconnect for two-dimensional ultrasound arrays," *IEEE Trans. Ultrason., Ferroelect., Freq. Contr.*, vol. 47, pp. 764–770, 2000.

[11] R. G. Swartz and J. D. Plummer, "Integrated silicon-PVF2 acoustic transducer arrays," *IEEE Trans. Ultrason., Ferroelect., Freq. Contr.*, vol. 26, pp. 1921–1931, 1979.

[12] J. H. Mo, A. L. Robinson, D. W. Fitting, F. L. Terry, and P. L. Carson, "Micromachining for improvement of integrated ultrasonic transducer sensitivity," *IEEE Trans. Ultrason., Ferroelect., Freq. Contr.*, vol. 37, pp. 134–139, 1990.

[13] K. Erikson, A. Hairston, A. Nicoli, J. Stockwell, and T. A. White, "A 128×128 ultrasonic transducer hybrid array," in *Proc. IEEE Ultrason. Symp.*, 1997, pp. 1625–1629.

[14] S. Calmes, C. H. Cheng, F. L. Degertekin, X. C. Jin, S. Ergun, and B. T. Khuri-Yakub, "Highly integrated 2-D capacitive micromachined ultrasonic transducers," in *Proc. IEEE Ultrason. Symp.*, 1999, pp. 1163–1166.

[15] O. Oralkan, X. C. Jin, F. L. Degertekin, and B. T. Khuri-Yakub, "Simulation and experimental characterization of a 2-D, 3MHZ capacitive micromachined ultrasonic transducer (CMUT) array element," in *Proc. IEEE Ultrason. Symp.*, 1999, pp. 1141–1144.

[16] A. G. Buck and R. A. Olson, "Ultrasound imaging probe assembly," U.S. Patent 6030346, 2000.

[17] J. A. Jensen and N. B. Svendsen, "Calculation of pressure fields from arbitrarily shaped, apodized, and excited ultrasound transducers," *IEEE Trans. Ultrason., Ferroelect., Freq. Contr.*, vol. 39, pp. 262–267, 1992.

[18] R. Krimholtz, D. A. Leedom, and G. L. Matthaei, "New equivalent circuits for elementary piezoelectric transducers," *Electron. Lett.*, vol. 6, pp. 398–399, 1970.

[19] R. E. Davidsen and S. W. Smith, "Two-dimensional arrays for medical ultrasound using multi-layer flexible circuit interconnection," *IEEE Trans. Ultrason., Ferroelect., Freq. Contr.*, vol. 45, pp. 338–348, 1998.

[20] S. W. Smith, P. D. Lopath, D. B. Adams, and G. P. Walcott, "Cardiac ultrasound phantom using a porcine heart model," *Ultrasound Med. Biol.*, vol. 21, pp. 693–697, 1995.

[21] C. B. Kim, R. Kesten, M. Javier, M. Hayase, A. S. Walton, M. E. Billingham, R. Kernoff, and S. N. Oesterle, "Percutaneous method of laser transmyocardial revascularization," *Catheter. Cardiovasc. Diag.*, vol. 40, pp. 223–228, 1997.

[22] M. K. Hong, R. Kornowski, M. B. Leon, Y. Gao, and E. Smith, "Acute effects of percutaneous direct myocardial revascularization with biosense holmium: YAG laser system," *J. Amer. Coll. Cardiol.*, vol. 32, Suppl. A, p. 307A, 1998.

[23] C. G. Hughes, S. S. Biswas, B. L. Yin, O. V. Baklanov, T. R. Degrado, R. E. Coleman, C. L. Donovan, J. E. Lowe, K. P. Landolfo, and B. H. Annex, "Intramyocardial but not intravenous vascular endothelial growth factor improves regional perfusion in hibernating porcine myocardium," *Circulation*, vol. 100, Suppl. S, no. 18, p. 2510, 1999.

Warren Lee (S'01) was born in Orange County, California, on September 27, 1976. He received B.S.E. degrees in biomedical and electrical engineering from Duke University in Durham, North Carolina, in 1998.

Currently he is a biomedical engineering doctoral candidate at Duke University. His current research involves the design and fabrication of two-dimensional array intracardiac transducers for real-time volumetric ultrasound imaging.

Stephen W. Smith (M'91) was born in Covington, Kentucky, on July 27, 1947. He received the B.A. degree in physics (summa cum laude) in 1967 from Thomas More College, Ft. Mitchell, Kentucky, the M.S. degree in physics in 1969 from Iowa State University, Ames, and the Ph.D. degree in biomedical engineering in 1975 from Duke University, Durham, North Carolina.

In 1969, he became a commissioned officer in the U.S. Public Health Service, assigned to the Food and Drug Administration, Center for Devices and Radiological Health, Rockville, Maryland, where he worked until 1990 in the study of medical imaging, particularly diagnostic ultrasound, and in the development of performance standards for such equipment. In 1978, he became an adjunct associate professor of radiology at Duke University Medical Center. In 1990, he became associate professor of biomedical engineering and radiology, and Director of Undergraduate Studies in Biomedical Engineering at Duke University. He holds 16 patents in medical ultrasound and has authored 100+ publications in the field.

Dr. Smith is cofounder of Volumetrics Medical Imaging. He has served on the education committee of the American Institute of Ultrasound in Medicine, the executive board of the American Registry of Diagnostic Medical Sonographers, the editorial board of *Ultrasonic Imaging*, and the Technical Program Committee of IEEE-UFFC. He was corecipient of the American Institute of Ultrasound in Medicine Matzuk Award in 1988 and 1990 and corecipient of the IEEE-UFFC Outstanding Paper Award in 1983 and 1994.